

# Coupling Identical 1D Many-Body Localized Systems

Pranjal Bordia,<sup>1,2</sup> Henrik P. Lüschen,<sup>1,2</sup> Sean S. Hodgman,<sup>1,2</sup>  
Michael Schreiber,<sup>1,2</sup> Immanuel Bloch,<sup>1,2</sup> and Ulrich Schneider<sup>1,2,3</sup>

<sup>1</sup>Fakultät für Physik, Ludwig-Maximilians-Universität München, Schellingstr. 4, 80799 Munich, Germany

<sup>2</sup>Max-Planck-Institut für Quantenoptik, Hans-Kopfermann-Str. 1, 85748 Garching, Germany

<sup>3</sup>Cavendish Laboratory, University of Cambridge,

J. J. Thomson Avenue, Cambridge CB3 0HE, United Kingdom

(Dated: May 30, 2022)

We experimentally study the effects of coupling one-dimensional Many-Body Localized (MBL) systems with identical disorder. Using a gas of ultracold fermions in an optical lattice, we artificially prepare an initial charge density wave in an array of 1D tubes with quasi-random onsite disorder and monitor the subsequent dynamics over several thousand tunneling times. We find a strikingly different behavior between MBL and Anderson Localization. While the non-interacting Anderson case remains localized, in the interacting case any coupling between the tubes leads to a delocalization of the entire system.

*Introduction.*—Many-Body Localization (MBL) marks a new paradigm in condensed matter and statistical physics. It describes an insulating phase in which a disordered, interacting many-body quantum system fails to act as its own heat bath [1–5]. In isolation, these systems will never achieve local thermal equilibrium and conventional statistical physics approaches break down. Unlike other insulating phases, MBL is not limited to ground states but can even occur in all excited states of a disordered many-body system [6–10]. A dynamical phase transition separates the MBL phase from conventional ergodic phases [11, 12], in which the isolated system thermalizes. In these ergodic phases, any initial quantum information becomes rapidly diluted in the exponentially large Hilbert space, leading to decoherence. In contrast, in the localized insulating phase quantum information can persist locally for an infinite amount of time [5]. This could potentially render quantum information devices less susceptible to noise and disorder. For many decades it remained unclear whether such a localized phase could persist in a many-body system beyond the non-interacting limit of an Anderson insulator [13]. Today, both theory and experiment have shown evidence for the existence of an MBL phase in interacting 1D systems [5–7, 14, 15]. Nonetheless, many fundamental questions regarding this phase and the associated phase transition as well as its extension to higher dimensions remain open, making it a highly active topic of current theoretical and experimental research.

One crucial requirement for the existence of a MBL phase is that no coupling to any external heat bath or bath-like structure exists. Any such coupling will eventually thermalize the system and ultimately destroy the non-thermalizing MBL phase [5, 16–19]. Since any experimental system will inevitably be coupled—albeit potentially very weakly—to an environment, it is of critical importance to quantitatively understand the effect of such a coupling. Furthermore, studying the effects of weak couplings can help to experimentally identify an MBL

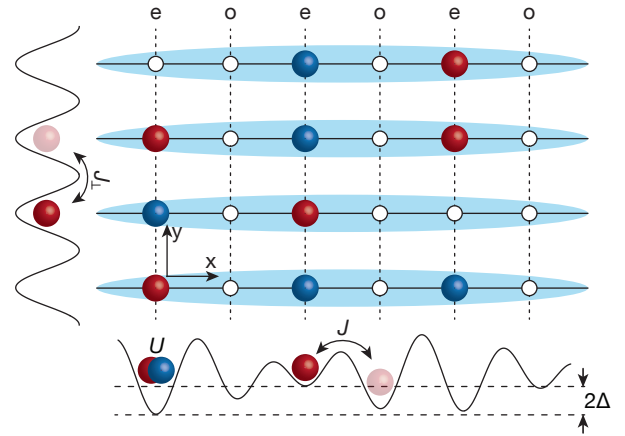


FIG. 1. Coupling identical MBL systems: A charge density wave (CDW) with atoms only occupying even sites ( $e$ ) is prepared in each of the identically disordered 1D tubes along the longitudinal ( $x$ ) direction, with hopping  $J$ , on-site interaction energy  $U$  and disorder strength  $\Delta$ . Red and blue spheres indicate a typical distribution of  $|\uparrow\rangle$  and  $|\downarrow\rangle$  atoms. We monitor the time evolution of such a state for different inter-tube coupling strengths  $J_{\perp}$ , that is different hopping amplitudes along the transverse ( $y$ ) direction.

phase and distinguish it from glasses or non-interacting Anderson localized phases.

Ultracold quantum gases in optical lattices form an ideal system to investigate these questions, as they are almost perfectly isolated from the external world and are highly controllable. Earlier experiments have investigated the interplay between disorder and interactions in the ground state of an isolated systems of ultracold bosons in optical lattices [20–22] and studied the influence of disorder on transport properties for lattice fermions [23]. Recently, we were able to show that for a wide range of energy-densities and interactions, an MBL phase exists in 1D Hubbard type chains with quasi-random disorder [14].

In this work, we experimentally study the effects of coupling identically disordered 1D MBL systems to each other. In particular, the disordered Hamiltonian is identical for all 1D tubes, but the initial configuration of atoms differs between the tubes (Fig. 1). We find that the coupled systems can collectively serve as a bath for each other, i.e. coupling localized systems can result in delocalizing all of them.

*Experiment.*—Our experiments start with a two component Fermi gas of  $^{40}\text{K}$  atoms in an equal mixture of the two lowest hyperfine states  $|F, m_F\rangle = |\frac{9}{2}, -\frac{9}{2}\rangle \equiv |\downarrow\rangle$  and  $|\frac{9}{2}, -\frac{7}{2}\rangle \equiv |\uparrow\rangle$  with a total atom number of about  $110\text{--}150 \times 10^3$  atoms. In the initial dipole trap, the atoms are at a temperature of  $0.19(2) T_F$ , where  $T_F$  is the Fermi temperature. We load the Fermi gas into the lowest band of a deep, three-dimensional simple cubic optical lattice, where tunneling can be neglected. Along the longitudinal ( $x$ ) direction, we then add a second (short) lattice (wavelength  $\lambda_s=532$  nm) to the initial (long) lattice (wavelength  $\lambda_l=1064$  nm). By controlling the phase of the short lattice during loading, we prepare a period-two ‘Charge-Density-Wave’ (CDW), where only even sites are occupied in the  $20 E_r$  deep short lattice. Here, the recoil energy is denoted by  $E_r = \hbar^2/2m\lambda^2$ , where  $\hbar$  is Planck’s constant,  $\lambda$  is the lattice wavelength and  $m$  is the atomic mass. The orthogonal lattices along  $y$  and  $z$  with a wavelength of  $\lambda_\perp=738$  nm are initially ramped up to  $45 E_r$ , creating an array of (almost) isolated 1D tubes. During lattice loading the interactions are kept strongly repulsive at a scattering length of  $a \approx 140 a_0$ , where  $a_0$  is the Bohr radius, by employing a Feshbach resonance centred at  $202.1$  G [24]. This results in a doublon fraction, that is the fraction of atoms on doubly occupied lattice sites, of  $\leq 10\%$ .

After the preparation of the CDW in the deep lattices, the desired interactions for the ensuing evolution are set. Additionally, an incommensurate lattice of wavelength  $\lambda_d=738$  nm is superimposed along the  $x$  direction to create quasi-random onsite disorder along the longitudinal direction. The system size is approximately 200 sites in the longitudinal and 120 sites in the transverse direction, and the central longitudinal tubes contains about 90 atoms [25]. After this preparation, the long lattice is quickly ramped to zero, the transverse  $y$  lattice is ramped to its final value, which controls the transverse coupling  $J_\perp$ , and the short lattice is reduced to  $8 E_r$ . This last ramp enables tunneling along the tube and thereby initiates the dynamics. After a variable evolution time, we extract the imbalance between atoms on even and odd sites  $\mathcal{I} = (N_e - N_o)/(N_e + N_o)$  [14]. Here  $N_e$  and  $N_o$  denote the population of even and odd sites respectively along the longitudinal direction and are extracted by mapping them to different bands of the superlattice [26].

The imbalance provides a measure of ergodicity breaking: because it quickly decays to zero under any ergodic dynamics, any non-zero imbalance persisting at

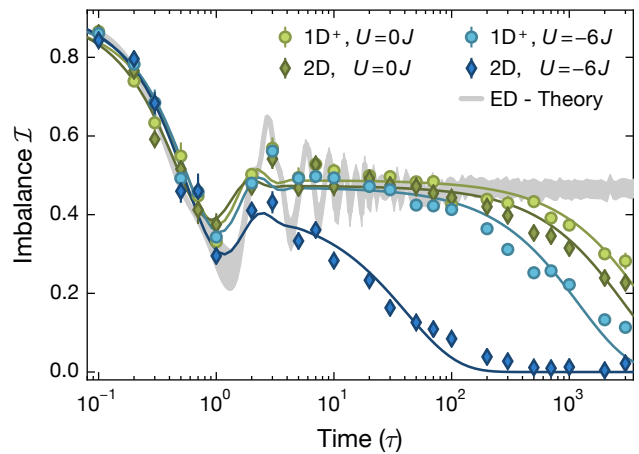


FIG. 2. Time evolution of a charge-density wave (CDW): An initially prepared 1D CDW evolves in a disordered system with disorder strength  $\Delta = 5 J$  along one axis. We measure the imbalance  $\mathcal{I}$  after a given evolution time in  $1\text{D}^+$  (circles) and  $2\text{D}$  (diamonds). Each data point is the average of 6 disorder phase realizations, with errorbars showing the standard error of the mean. Solid lines are fits [25] from which we extract the imbalance lifetimes. Shown in grey is an exact diagonalization (ED) calculation for  $J_\perp = 0$ ,  $\Delta = 5 J$  and  $U = 0$  [25].

long times signifies a memory of the initial state and directly indicates localization [14, 27].

*Model.*—Our system consists of an array of 1D tubes with identical quasi-random on-site disorder along the longitudinal direction. Each tube can be described by the Aubry-André Model [28] with interactions [29], as depicted in Fig. 1. A finite hopping amplitude  $J_\perp$  along the transverse ( $y$ ) direction introduces a coupling between adjacent tubes. The Hamiltonian of the system is given by

$$\begin{aligned} \hat{H} = & -J \sum_{i,j,\sigma} (\hat{c}_{i+1,j,\sigma}^\dagger \hat{c}_{i,j,\sigma} + \text{h.c.}) \\ & -J_\perp \sum_{i,j,\sigma} (\hat{c}_{i,j+1,\sigma}^\dagger \hat{c}_{i,j,\sigma} + \text{h.c.}) \\ & + \Delta \sum_{i,j,\sigma} \cos(2\pi\beta i + \phi) \hat{n}_{i,j,\sigma} + U \sum_{i,j} \hat{n}_{i,j,\uparrow} \hat{n}_{i,j,\downarrow}, \end{aligned} \quad (1)$$

where  $J \approx \hbar \times 500$  Hz is the tunneling matrix element between neighboring sites along a tube and  $J_\perp$  denotes the transverse ( $y$ ) hopping between the tubes. The creation (annihilation) operator for a fermion in spin state  $\sigma \in \{\uparrow, \downarrow\}$  on site  $i$  in tube  $j$  is  $\hat{c}_{i,j,\sigma}^\dagger$  ( $\hat{c}_{i,j,\sigma}$ ) and the local number operator is given by  $\hat{n}_{i,j,\sigma} = \hat{c}_{i,j,\sigma}^\dagger \hat{c}_{i,j,\sigma}$ . The quasi-random on-site disorder is characterized by the disorder amplitude  $\Delta$ , the incommensurable wavelength ratio  $\beta = \lambda_s/\lambda_d$  and the relative phase  $\phi$ . Finally, the on-site interaction energy is given by  $U$ .

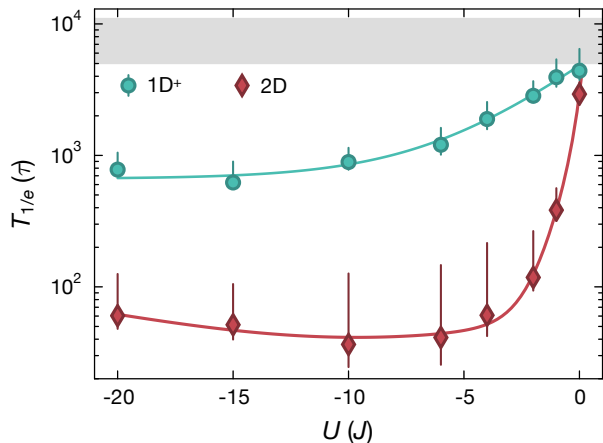


FIG. 3. Imbalance lifetimes versus interactions ( $U$ ): Imbalance lifetimes at  $\Delta = 5J$  for  $1D^+$  and  $2D$ . The lifetimes were extracted from fits to time traces such as in Fig. 2. Errorbars indicate the uncertainty in the fitting procedure [25]. The gray shaded area indicates the range of measured atom number lifetimes, while the lines are guides to the eye.

In the limit  $J_{\perp} \rightarrow 0$ , the system decouples into many one-dimensional tubes, which show many-body localization [14]. For our experiment, the accessible limits of almost zero coupling  $J_{\perp} \lesssim 10^{-3}J$  and equal coupling  $J_{\perp} = J$  are termed the  $1D^+$  and  $2D$  cases, respectively.

*Results.*—We monitor the time evolution of the imbalance at disorder amplitude  $\Delta = 5J$  for various interaction strengths  $U$  in both the  $1D^+$  and  $2D$  cases. This disorder strength is deep in the MBL regime for isolated  $1D$  tubes. Fig. 2 shows exemplary time traces at  $U = 0$  and  $U = -6J$ , with all times given in units of the longitudinal tunneling time  $\tau = \hbar/J$ . We start with an out-of-equilibrium density wave with an initial imbalance of  $\mathcal{I}(t=0) = 0.91 \pm 0.03$  and observe a fast initial decrease of the imbalance up to approximately one tunneling time. This decrease is similar in all cases and corresponds to an initial relaxation in the longitudinal direction.

In both non-interacting cases, the initial decrease is followed by highly damped oscillations around a plateau at finite imbalance, closely matching the expected steady state for this Anderson localized system [14, 25]. At very long times ( $\gg 100\tau$ ), the curves start to deviate from this plateau and exhibit a slow decay. The corresponding lifetime is extracted by fitting the imbalance traces to a damped sinusoid, which models the initial fast relaxation, times a second exponential to capture the slow decay [25]. In the absence of interactions, the observed long time dynamics is dominated by classical noise, photon scattering from lattice beams and other technical imperfections. These processes couple the system to the environment and over time delocalize it [30, 31]. In addition, these experimental imperfections also give rise to an atom number decay, which limits the lifetime of atoms

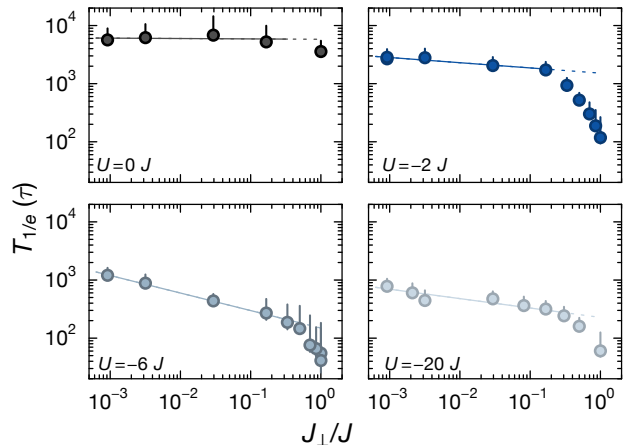


FIG. 4. Imbalance lifetimes in the  $1D$ - $2D$  crossover: The coupling strength  $J_{\perp}$  between adjacent tubes is varied continuously for  $\Delta = 5J$  at four different interactions  $U$ . Here  $J_{\perp}/J \lesssim 10^{-3}$  and  $J_{\perp}/J = 10^0$  correspond to the  $1D^+$  and the  $2D$  cases respectively. The lack of saturation as  $J_{\perp} \rightarrow 0$  indicates that the residual inter-tube coupling still limits the imbalance lifetime in the  $1D^+$  case. Solid lines denote power-law fits  $\propto J_{\perp}^k$  for small  $J_{\perp}$ , with fitted exponents  $k(U)$  of  $k(0) = 0.00(4)$ ,  $k(-2) = -0.09(2)$ ,  $k(-6) = -0.30(1)$  and  $k(-20) = -0.16(3)$  [25]. We note that in principle the tunneling along the  $z$  direction becomes sizeable for the smallest  $J_{\perp}$ , as  $J_{\perp}^z/J \sim 10^{-3}$ .

in the lattice to  $0.5 - 1.1 \times 10^4 \tau$  [25]. This range of atom number lifetimes is indicated by the grey shaded region in Fig. 3, the lower bound of which approximately coincides with the non-interacting imbalance lifetimes, indicating the relevance of technical imperfections on this timescale. In the absence of interactions, the observed dynamics in  $1D^+$  and  $2D$  are almost the same, since the disorder potential is identical in all tubes [25]. Therefore the  $2D$  system is separable, and the longitudinal and transverse directions are decoupled. Note that we do not expect this to hold if the disorder were different in different tubes [32].

Adding interactions, however, breaks the separability of the system and the transverse dynamics can now affect the imbalance along the longitudinal direction. Since there is no disorder along the transverse direction, particles are free to move along this direction. In the interacting case, this couples the originally localized tubes such that they collectively act as a bath for each other and thereby delocalize the entire system. As a consequence, the interacting  $2D$  trace in Fig. 2 displays no plateau but instead shows a fast decay. To understand this behavior further, we map out the imbalance lifetimes in the  $1D^+$  and  $2D$  cases for various interaction strengths (Fig. 3). We find that in  $2D$ , even small interactions are sufficient to dramatically reduce the imbalance lifetime to less than  $100\tau$ . This is consistent with ergodic dynamics and demonstrates the absence of MBL in this case.

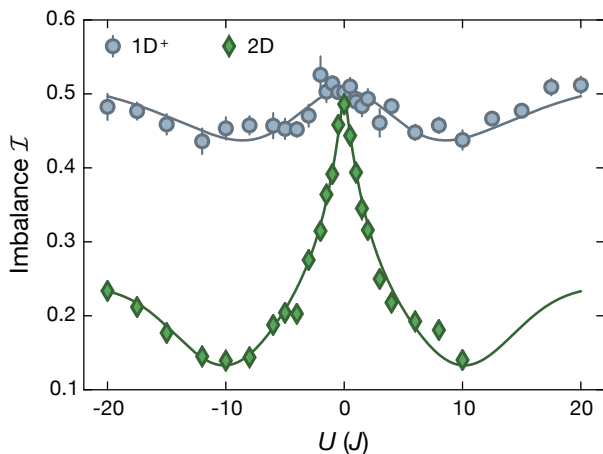


FIG. 5. Imbalance vs. interactions ( $U$ ) at fixed times: Data taken at  $\Delta = 5J$  averaged over three different times ( $38\tau - 41\tau$ ) and 4 disorder phases  $\phi$ . In the  $1D^+$  case (circles), the imbalance corresponds to the stationary value [14], whereas in the 2D case (diamonds) it is indicative of the decay lifetime. Solid lines are guides to the eye. The 2D case is limited to  $U/J \leq 10$  due to details of the used Feshbach resonance [24].

*1D-2D Crossover.*—Although MBL is expected to be stable in the isolated 1D case, the  $1D^+$  data in Fig. 3 shows a qualitatively similar behavior to the 2D case, but with a much weaker decrease of imbalance lifetimes with increasing interactions. This suggests that the small but non-zero transverse coupling also limits the lifetimes in the  $1D^+$  case. In order to test this, we vary the strength of the inter-tube coupling between the 2D and the  $1D^+$  limits for four different interactions (Fig. 4) and in all the interacting cases observe increasing lifetimes for decreasing coupling strengths  $J_{\perp}$ . For small but finite coupling strengths, we observe a linear trend on a log-log scale (Fig. 4), suggesting a power law dependence. For strong intertube coupling ( $J_{\perp} \approx J$ ), there is a crossover to a faster decay. The fitted exponents are surprisingly small ( $< 1$ ) and depend non-monotonically on the interactions. In the non-interacting limit  $U \rightarrow 0$ , the lifetimes are on the order of the atom number lifetime and are independent of transverse coupling due to the separability of the problem. This highlights the striking difference between MBL and Anderson localization.

Extrapolating towards the limit of the true 1D case ( $J_{\perp} \rightarrow 0$ ), we would expect the lifetimes of the interacting system to saturate once the inter-tube coupling is no longer the dominant decay mechanism. However, in the experimentally accessible regime we cannot observe any signs of saturation, strongly suggesting that the interacting lifetimes are still limited by the non-zero residual transverse coupling to the neighboring tubes, even in the  $1D^+$  case.

*Constant evolution time.*—The interaction dependence is also visible in the imbalance value measured after a

fixed evolution time of around  $40\tau$ , as shown in Fig. 5. We observe a substantial decrease of the 2D imbalance with small interactions, which is consistent with the sharply decreasing lifetimes. Additionally, Fig. 5 shows that the dynamics are symmetric around  $U = 0$ , which is expected due to a dynamical symmetry of the Fermi-Hubbard Model [33]. Interestingly, we observe an increasing imbalance in the 2D data for strong interactions. We checked that this increase is not due to doublons by removing any residual doublons with a pulse of near-resonant light [34] prior to the evolution. This increase in lifetime might be due to the reduced phase space for scattering in the hard-core limit ( $U \gg J$ ). A recent theoretical study using a cluster expansion method on a smaller system ( $8 \times 8$  sites) observed a similar trend [35].

At  $40\tau$ , the  $1D^+$  case is dominated by the 1D plateau value and shows the characteristic ‘W’ shape of the steady state imbalance of the MBL system [14], with little influence from the (much longer) lifetimes. As shown in the supplementary material [25], we additionally find that the imbalance lifetime in all cases depends strongly on the disorder strength and is ultimately limited by the atom number lifetime.

*Conclusion.*—We have studied the stability of many-body localized 1D systems under an inter-tube coupling. We found that even weak couplings have a delocalizing effect on the MBL phase, while leaving the non-interacting Anderson limit unchanged. This highlights the differences between these two regimes and shows the principal fragility of MBL with respect to coupling to any external heat bath [5, 16–19]. Furthermore, we have not observed any saturation in imbalance lifetimes even for the smallest couplings we could attain, indicating that this inter-tube coupling is the dominant decay mechanism in the current MBL experiment. Nonetheless, the achieved lifetimes of several thousand tunneling times already vastly exceed the lifetimes of typical many-body states, such as e.g. superfluid states in optical lattices. This demonstrates the stability of MBL with respect to other experimental imperfections and increases the prospects of realizing localization protected order [36–38] and applications in quantum-information [5].

An important next step will be to extend this study to the ‘true’ 2D case with disorder along both directions. In addition, future experiments should also be able to address the question of the stability of MBL under external influences, such as photon scattering [30, 39] and time-dependent modulations [40, 41].

We acknowledge useful discussions with E. Altman, E. Demler, M. Fischer, D. Huse, M. Knapp, R. Nandkishore and A. Pal. We acknowledge financial support by the European Commission (UQUAM, AQUUS) and the Nanosystems Initiative Munich (NIM).

- 
- [1] J. M. Deutsch, “Quantum statistical mechanics in a closed system,” *Phys. Rev. A* **43**, 2046–2049 (1991).
- [2] Mark Srednicki, “Chaos and quantum thermalization,” *Phys. Rev. E* **50**, 888–901 (1994).
- [3] M. Rigol, V. Dunjko, and M. Olshanii, “Thermalization and its mechanism for generic isolated quantum systems,” *Nature* **452** (2008).
- [4] Anatoli Polkovnikov, Krishnendu Sengupta, Alessandro Silva, and Mukund Vengalattore, “*Colloquium* : Nonequilibrium dynamics of closed interacting quantum systems,” *Rev. Mod. Phys.* **83**, 863–883 (2011).
- [5] Rahul Nandkishore and David A. Huse, “Many-body localization and thermalization in quantum statistical mechanics,” *Annual Review of Condensed Matter Physics* **6**, 15–38 (2015).
- [6] D.M. Basko, I. L. Aleiner, and B. L. Altshuler, “Metal-insulator transition in a weakly interacting many-electron system with localized single-particle states,” *Ann. Phys.* **321** (2006).
- [7] I. V. Gornyi, A. D. Mirlin, and D. G. Polyakov, “Interacting electrons in disordered wires: Anderson localization and low- $t$  transport,” *Phys. Rev. Lett.* **95**, 206603 (2005).
- [8] Vadim Oganesyan and David A. Huse, “Localization of interacting fermions at high temperature,” *Phys. Rev. B* **75**, 155111 (2007).
- [9] John Z. Imbrie, “On many-body localization for quantum spin chains,” (2014), arXiv:1403.7837.
- [10] V.P. Michal, I.L. Aleiner, B.L. Altshuler, and G.V. Shlyapnikov, “Finite-temperature fluid-insulator transition of strongly interacting 1d disordered bosons,” (2015), arXiv:1502.00282.
- [11] Arijeet Pal and David A. Huse, “Many-body localization phase transition,” *Phys. Rev. B* **82**, 174411 (2010).
- [12] Ronen Vosk and Ehud Altman, “Many-body localization in one dimension as a dynamical renormalization group fixed point,” *Phys. Rev. Lett.* **110**, 067204 (2013).
- [13] P. W. Anderson, “Absence of diffusion in certain random lattices,” *Phys. Rev.* **109**, 1492–1505 (1958).
- [14] Michael Schreiber, Sean S. Hodgman, Pranjal Bordia, Henrik P. Lschen, Mark H. Fischer, Ronen Vosk, Ehud Altman, Ulrich Schneider, and Immanuel Bloch, “Observation of many-body localization of interacting fermions in a quasirandom optical lattice,” *Science* **349**, 842–845 (2015).
- [15] Ehud Altman and Ronen Vosk, “Universal dynamics and renormalization in many-body-localized systems,” *Annual Review of Condensed Matter Physics* **6**, 383–409 (2015).
- [16] N. F. Mott, “Conduction in non-crystalline materials,” *Philosophical Magazine* **19**, 835–852 (1969).
- [17] Rahul Nandkishore, Sarang Gopalakrishnan, and David A. Huse, “Spectral features of a many-body-localized system weakly coupled to a bath,” *Phys. Rev. B* **90**, 064203 (2014).
- [18] Sonika Johri, Rahul Nandkishore, and R. N. Bhatt, “Many-body localization in imperfectly isolated quantum systems,” *Phys. Rev. Lett.* **114**, 117401 (2015).
- [19] David A. Huse, Rahul Nandkishore, Francesca Pietracaprina, Valentina Ros, and Antonello Scardicchio, “Localized systems coupled to small baths: From anderson to zeno,” *Phys. Rev. B* **92**, 014203 (2015).
- [20] B. Deissler, M. Zaccanti, G. Roati, C. D’Errico, M. Fattori, M. Modugno, G. Modugno, and M. Inguscio, “Delocalization of a disordered bosonic system by repulsive interactions,” *Nature Physics* **6**, 354–358 (2010).
- [21] Bryce Gadway, Daniel Pertot, Jeremy Reeves, Matthias Vogt, and Dominik Schneble, “Glassy behavior in a binary atomic mixture,” *Phys. Rev. Lett.* **107**, 145306 (2011).
- [22] Chiara D’Errico, Eleonora Lucioni, Luca Tanzi, Lorenzo Gori, Guillaume Roux, Ian P. McCulloch, Thierry Giamarchi, Massimo Inguscio, and Giovanni Modugno, “Observation of a disordered bosonic insulator from weak to strong interactions,” *Phys. Rev. Lett.* **113**, 095301 (2014).
- [23] S. S. Kondov, W. R. McGehee, W. Xu, and B. DeMarco, “Disorder-induced localization in a strongly correlated atomic hubbard gas,” *Phys. Rev. Lett.* **114**, 083002 (2015).
- [24] C. A. Regal, C. Ticknor, J. L. Bohn, and D. S. Jin, “Creation of ultracold molecules from a fermi gas of atoms,” *Nature* **424** (2003).
- [25] See Supplementary Material for details.
- [26] S. Trotzky, Y-A. Chen, A. Flesch, I. P. McCulloch, U. Schollwoeck, J. Eisert, and I. Bloch, “Probing the relaxation towards equilibrium in an isolated strongly correlated one-dimensional bose gas,” *Nat. Phys.* **8** (2012).
- [27] Rubem Mondaini and Marcos Rigol, “Many-body localization and thermalization in disordered hubbard chains,” (2015), arXiv:1508.02722.
- [28] S. Aubry and G. André, “Analyticity breaking and anderson localization in incommensurate lattices,” *Ann. Israel Phys. Soc.* **3** (1980).
- [29] Shankar Iyer, Vadim Oganesyan, Gil Refael, and David A. Huse, “Many-body localization in a quasiperiodic system,” *Phys. Rev. B* **87**, 134202 (2013).
- [30] S. A. Gurvitz, “Delocalization in the anderson model due to a local measurement,” *Phys. Rev. Lett.* **85**, 812–815 (2000).
- [31] Boris Nowak, Jami J. Kinnunen, Murray J. Holland, and Peter Schlagheck, “Delocalization of ultracold atoms in a disordered potential due to light scattering,” *Phys. Rev. A* **86**, 043610 (2012).
- [32] E. Abrahams, P. W. Anderson, D. C. Licciardello, and T. V. Ramakrishnan, “Scaling theory of localization: Absence of quantum diffusion in two dimensions,” *Phys. Rev. Lett.* **42**, 673–676 (1979).
- [33] U. Schneider, L. Hackermüller, J. P. Ronzheimer, S. Will, S. Braun, T. Best, I. Bloch, E. Demler, S. Mandt, D. Rasch, and A. Rosch, “Fermionic transport and out-of-equilibrium dynamics in a homogeneous hubbard model with ultracold atoms,” *Nat. Phys.* **8** (2012).
- [34] J. P. Ronzheimer, M. Schreiber, S. Braun, S. S. Hodgman, S. Langer, I. P. McCulloch, F. Heidrich-Meisner, I. Bloch, and U. Schneider, “Expansion dynamics of interacting bosons in homogeneous lattices in one and two dimensions,” *Phys. Rev. Lett.* **110**, 205301 (2013).
- [35] M. D. Reichl and E. J. Mueller, “Dynamics of pattern-loaded fermions in bichromatic optical lattices,” (2015), arXiv:1508.00472.
- [36] David A. Huse, Rahul Nandkishore, Vadim Oganesyan, Arijeet Pal, and S. L. Sondhi, “Localization-protected quantum order,” *Phys. Rev. B* **88**, 014206 (2013).
- [37] Bela Bauer and Chetan Nayak, “Area laws in a many-

- body localized state and its implications for topological order,” *Journal of Statistical Mechanics: Theory and Experiment* **2013**, P09005 (2013).
- [38] Anushya Chandran, Vedika Khemani, C. R. Laumann, and S. L. Sondhi, “Many-body localization and symmetry-protected topological order,” *Phys. Rev. B* **89**, 144201 (2014).
- [39] Boris Nowak, Jami J. Kinnunen, Murray J. Holland, and Peter Schlagheck, “Delocalization of ultracold atoms in a disordered potential due to light scattering,” *Phys. Rev. A* **86**, 043610 (2012).
- [40] S. Gopalakrishnan, M. Mueller, V. Khemani, M. Knap, E. Demler, and D.A. Huse, (2015), arXiv:1502.07712.
- [41] Kartiek Agarwal, Sarang Gopalakrishnan, Michael Knap, Markus Müller, and Eugene Demler, “Anomalous diffusion and griffiths effects near the many-body localization transition,” *Phys. Rev. Lett.* **114**, 160401 (2015).
- [42] U. Schneider, L. Hackermüller, S. Will, Th. Best, I. Bloch, T. A. Costi, R. W. Helmes, D. Rasch, and A. Rosch, “Metallic and insulating phases of repulsively interacting fermions in a 3d optical lattice,” *Science* **322**, 1520–1525 (2008).

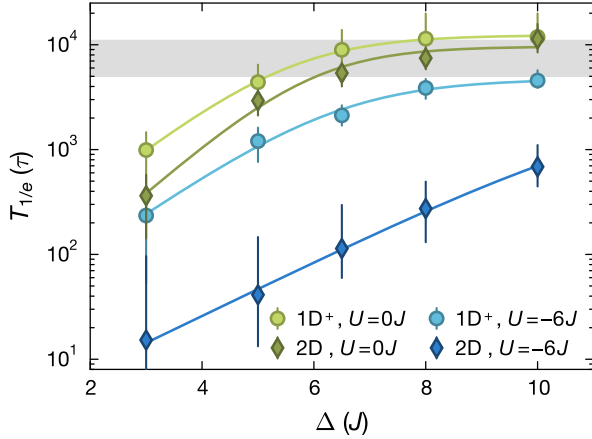


FIG. 6. Imbalance lifetimes as a function of disorder strength: The lifetimes were extracted by fits to individual time traces taken up to  $3000\tau$ , as in the main text. Errorbars indicate uncertainty in the fitting procedure. The gray shaded area indicates the range of typical atom number lifetimes. Solid lines show the results of saturated exponential fits described in the text.

### Supplementary Material

*Imbalance Lifetimes vs Disorder Strength.*—Fig. 6 shows the dependence of imbalance lifetimes on the disorder strength  $\Delta$  in the  $1D^+$  and the  $2D$  case for  $U = 0$  and for  $U = -6J$ . In all cases, we observe exponentially increasing lifetimes with larger  $\Delta$ . We attribute this to a reduced effectiveness of any bath-like perturbation for large disorder strengths. At long lifetimes this behaviour saturates, as the imbalance lifetimes approach the same order of magnitude as the atom loss lifetimes. Since all time traces in the paper are measured up to  $3000\tau$ , lifetimes exceeding  $5000\tau$  may be affected by systematic errors due to the fitting procedure becoming unreliable.

To capture the behavior with  $\Delta$  we fit the data with the following empirical function:

$$T_{1/e} = \frac{1}{\Gamma_b + ae^{-b\Delta}}, \quad (2)$$

where  $\Gamma_b$  represents the background imbalance loss due to noise, while  $a$  and  $b$  are free parameters. These fits are represented as solid lines in Fig. 6. The fit routine is performed in logarithmic units.

*Non-Interacting Lifetime Difference between  $1D^+$  and  $2D$ .*—The difference between the non-interacting  $1D^+$  and the  $2D$  data is most likely due to technical imperfections. Firstly, the interactions  $U$  may not be exactly zero for all times as it relies on the stability and the absolute calibration of the magnetic field. Secondly, the lattice beams have gaussian envelopes. This implies that both longitudinal hopping and disorder depend slightly

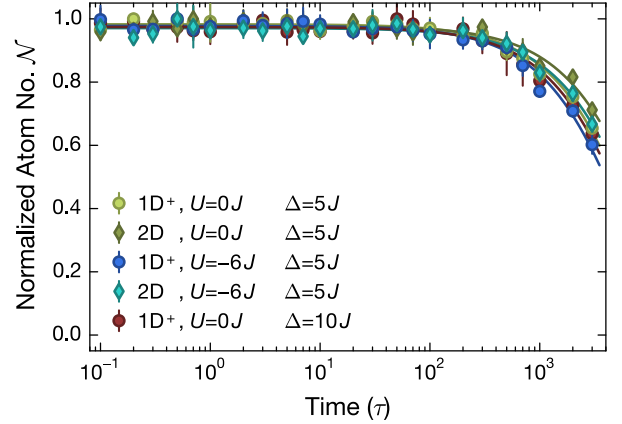


FIG. 7. Normalized atom loss time traces: Characteristic traces showing the loss of atoms for different couplings  $J_{\perp}$ , disorders  $\Delta$  and interactions  $U$ . Every data point is averaged over 6 disorder realizations  $\phi$ . Each trace was individually normalized to its maximum value after averaging. Errorbars show the error of the mean. Lines are fit with exponentials of the form  $Ae^{-t/T_a}$ .

on the transverse position. Thirdly, the relative phase of the disorder might be slightly different between neighbouring tubes due to slight misalignment between the disorder beam and the main lattice. These imperfections break the separability of the problem.

*Atom Number Lifetimes.*—In order to determine the atom number lifetime, we fit an exponential decay to the measured atom number time trace for every imbalance dataset. Five typical curves are shown in Fig. 7. The lifetimes are similar across the full investigated parameter range and we see no strong trend with either  $\Delta$  or  $U$ . Extracted lifetimes from the exponential fits lie in the range of  $0.5 - 1.1 \times 10^4 \tau$ .

As the experimental lifetime of atoms in the pure dipole trap is over  $10^5 \tau$ , the detected atom loss in the lattice must be dominated by off-resonant photon scattering of lattice photons as well as frequency and amplitude noise in the optical fields. This is consistent with the extracted atom number lifetimes being slightly higher in the  $2D$  cases as compared to the  $1D^+$  cases, as the total optical power in the lattice beams is lower in the  $2D$  cases. The loss channels formed by such processes will most likely involve excitations of atoms to higher bands. We note that, due to the long observed atom number lifetimes, these loss channels are unlikely to be relevant for the fast imbalance decay at the observed timescales in  $2D$ : Previous DMRG simulations in  $1D$  [14] agreed well with the experimental measurements in the  $1D^+$  case until  $\approx 100\tau$ . Hence, we do not expect higher bands to play a significant role up to at least this time. Furthermore, the atom number lifetimes in the  $2D$  cases are even slightly longer

than in the  $1D^+$  cases. Besides, at a relatively short time of  $40\tau$ , as presented in Fig. 5, we already find a strong effect of the inter-tube coupling, despite the fact that at these time scales there is no discernible atom loss.

*Extracting Imbalance Lifetimes.*—The observed time evolutions of the imbalance  $\mathcal{I}$  displays some common characteristic features. The imbalance starts close to unity, followed by a couple of oscillations with a period on the order of  $\tau$ , which quickly settle to a non-zero plateau value, before decaying to zero in the long-term limit. To quantify this long term decay we fit the sum of a damped sinusoidal and an offset multiplied with an overall exponential decay. This fitting function is given by:

$$\mathcal{I} = (Ae^{-t/t_1}\cos(\nu t) + I_{st})e^{-\Gamma t} \quad (3)$$

where  $A$  is the amplitude of the sinusoid with oscillation frequency  $\nu$  and oscillation damping time  $t_1 \sim \tau$ , the plateau value  $I_{st}$ , and the long-term decay rate  $\Gamma$ . From this fit function we obtain the lifetimes  $T_{1/e} = 1/\Gamma$ , as shown in Figs. 3, 4 and 6. This lifetime would diverge in the case of a perfectly localized system without external noise and strictly vanishing bath couplings.

The errorbars in  $T_{1/e}$  throughout the paper are an indication of the possible systematic errors inherent in the choice of the specific fit function. They are substantially larger than the fit uncertainty and indicate the total span of fit values obtained using the following different fit functions:

- Fitting Eqn. 3 and repeating the fits with fixed values of the offset  $I_{st}$  that are 0.03 above or below the previously fitted value
- Fitting  $e^{-\Gamma t}$  for the time ranges of  $4 - 3000\tau$  and  $50 - 3000\tau$
- Fitting  $e^{-\Gamma t} + o$  with  $o = \pm 0.02$  for the same time windows as above

*Exact Diagonalization.*—The ED calculations are adapted from our previous work. We simulate the Anderson localization limit by performing Exact Diagonalization (ED) on a single, non-interacting particle and account for our experimental setup by averaging over fifty phases (equally spaced between  $[0, 2\pi]$ ), the dipole trap, the inhomogeneity of the lattice and the atomic cloud shape. Full details of the ED can be found in Ref. [14].

*General Sequence.*—The experiment produces an ultracold gas of fermionic Potassium-40 ( $^{40}\text{K}$ ) atoms by sympathetically cooling  $^{40}\text{K}$  with bosonic Rubidium-87 ( $^{87}\text{Rb}$ ) in a plugged quadrupole trap followed by an optical dipole trap. Reducing the dipole trap depth lower

than a threshold value completely removes  $^{87}\text{Rb}$  due to its higher mass, such that only  $^{40}\text{K}$  remains in the trap. We further evaporate  $^{40}\text{K}$  in an equal mixture of the two lowest hyperfine states of the  $^4S_{1/2}$  manifold ( $|F, m_F\rangle = |9/2, -9/2\rangle \equiv |\downarrow\rangle$  and  $|9/2, -7/2\rangle \equiv |\uparrow\rangle$ ) to a final temperature of  $T/T_F = 0.19(0.02)$ , where  $T_F$  is the Fermi temperature. Interactions between the two states can be tuned via an s-wave Feshbach resonance centred at 202.1G [24]. The scattering length  $a$  is set to  $140a_0$  during lattice loading to avoid double occupancies. Here,  $a_0$  denotes the Bohr radius. The number of double occupancies are characterized by converting them into Feshbach molecules via crossing the Feshbach resonance and subsequently imaging the remaining single atoms [42].

After loading into the deep lattices (as described in the main text), we then set the scattering length to control the desired interactions  $U$  in the lattice for the following evolution time. At the end of this preparation stage, we ramp down the  $x$ -short lattice from  $20E_r$  to  $8E_r$  in  $10\mu\text{s}$  and ramp down the  $x$ -long lattice to  $0E_r$  in the same time. The disorder lattice is simultaneously ramped up to the desired disorder strength. The orthogonal  $y$ -lattice is ramped to the final value with an additional time of  $90\mu\text{s}$ . All of these lattice ramp times are short compared to a tunneling time  $\tau$ . The system is then allowed to evolve for various evolution times. For detection, the short lattice, the long lattice and the orthogonal lattices are ramped high again to inhibit hopping and freeze all occupations. Finally, we employ the bandmapping technique to obtain the number of atoms on the even and odd sites [26]. All bandmapping images are taken with 8ms time of flight and are imaged along the  $y$ -axis (i.e. orthogonal to the superlattice axis).

The cloud size in the lattice is measured via in-situ imaging. It can be described by a gaussian, with standard deviation  $\sigma$  of  $\sim 14\mu\text{m}$  and  $\sim 11\mu\text{m}$  in the  $x$  and  $y$  directions respectively. To estimate the number of sites in the central lattice tube, we take a value which corresponds to  $4\sigma$ , i.e. the range from  $-2\sigma$  to  $+2\sigma$ .

*Lattice Parameters.*—All lattice potentials result from retroreflected laser beams with gaussian intensity profiles and  $1/e^2$  radii (waists) of  $150\mu\text{m}$  that are centered at the position of the atoms. The lattice beams along the  $y$  and  $z$  direction and the disorder lattice light originate from the same Coherent MBR-110 Ti:Sa laser operated at 738 nm, which is locked to its internal reference cavity. In order to eliminate cross-interference between beams along different axes, separate beams have orthogonal polarizations and are shifted to different frequencies using acousto-optic modulators. The relative phase  $\phi$  of the disorder potential is controlled by slightly changing the frequency of this laser. The 1064 nm laser used for the long wavelength superlattice along the  $x$ -direction is locked to a dedicated reference cavity that is acoustically isolated and thermally stabilized to 65 kHz linewidth over 100 ms. A 532 nm Coherent Verdi laser is used as



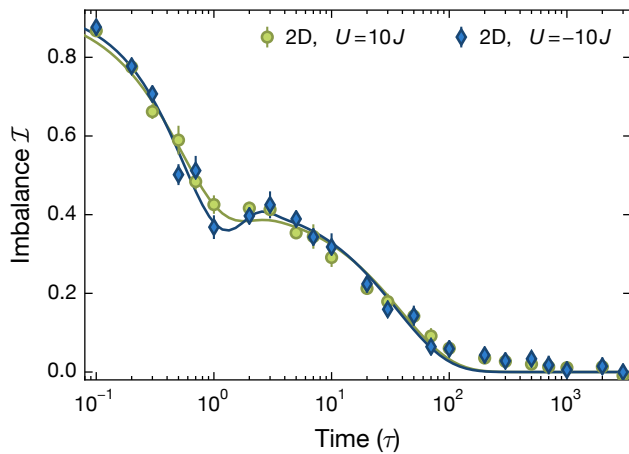


FIG. 8. Dynamical Symmetry of the Hubbard Model: Time traces showing the evolution of the imbalance  $\mathcal{I}$  in 2D for  $\Delta = 5 J$  and  $U = \pm 10 J$ . The data is identical within experimental scatter, showing that the decay of the imbalance does not depend on the sign of  $U$ . Each point is averaged over six disorder realizations  $\phi$ . Error bars denote the error of the mean.

the short lattice and is locked to frequency doubled light from the 1064 nm laser via an offset lock.

*Disorder Strength.*—The disorder strength  $\Delta$  depends on the lattice depth of the 532 nm laser (main lattice), the lattice depth of the disorder lattice and the ratio of their wavelengths  $\beta \approx 532/738$ . We use  $8 E_{r,532}$  as the main lattice depth, where  $E_{r,532} = h \times 17.64 \text{ kHz}$  is the recoil energy in the 532 nm lattice. The disorder strength is then given by  $\Delta/J = 6.67 s_d$ , where  $s_d$  is the depth of the disorder lattice in units of the 738 nm recoil energy. A complete derivation is provided in the supplementary material of [14].

*Dynamical  $U \leftrightarrow -U$  Symmetry.*—We load the atoms in the lattice at magnetic fields above the Feshbach resonance at 202.1 G [24]. On this side of the resonance, the maximum positive scattering length that can be obtained with our experiment is  $a \approx 142 a_0$ . This scattering length corresponds to an interaction strength of  $U \approx 12 J$  in the 2D case. However, there is no such restriction in the case of negative interactions. Hence we measure most of the data with attractive interactions (i.e.  $U$  negative). From a dynamical symmetry of the Hubbard model [33], we expect the dynamics to be identical for  $\pm U$ , as was observed to be the case for the short time behaviour in the 1D<sup>+</sup> case [14]. However, to investigate whether the symmetry also holds for the long term dynamics, we measure the time traces in the 2D case for  $U = \pm 10 J$ . This data is shown in Fig. 8 and indicates that the relaxation dynamics are indeed symmetric about  $U = 0$ . Since fluctuations of

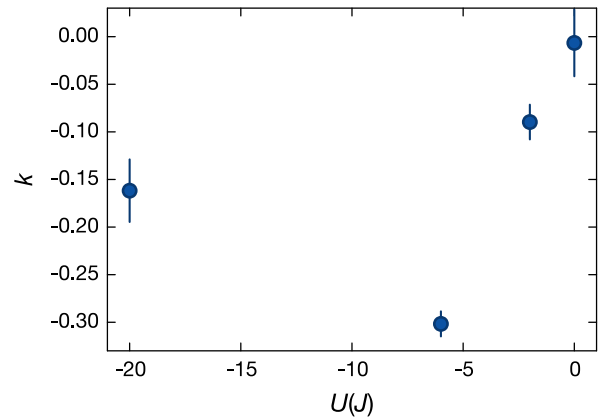


FIG. 9. Fitted Power Law Exponents for 1D-2D Crossover: Shown are the power law exponents of the 1D-2D crossover as a function of interaction strength. Error bars denote the fit error.

the magnetic field would cause much smaller changes of the scattering length in the  $U = +10 J$  case than in the  $U = -10 J$  case, the observed  $U \leftrightarrow -U$  symmetry indicates that neither field fluctuations nor the proximity to the Feshbach resonance contribute significantly to the decay of imbalance in the interacting 2D cases.

*Doublon Dependence.*—While all the data presented in this paper is taken with a rather small doublon fraction of  $\approx 8\%$ , we also briefly investigate the effect of doublons on the imbalance lifetimes. We measure the lifetimes in the 1D<sup>+</sup> and the 2D case at  $\Delta = 5 J$ ,  $U = -6 J$  for doublon fractions of 8% and 50% as well as for  $U = -20 J$  with 0% and 8% doublons. We can vary the doublon fraction between  $\approx 8\%$  to  $\approx 50\%$  by varying the scattering length during lattice loading between  $a_{\text{load}} = -140 a_0$  to  $+140 a_0$ . In addition, we can reduce the doublon fraction further to almost zero by applying a near resonant blast pulse in the deep lattice. This removes the leftover doublons while leaving the singly occupied sites unaffected. For all of the above cases, we observe less than 5% change in the imbalance lifetime, with slightly longer imbalance lifetimes for higher doublon fractions.

*Power-Law Fits for 1D-2D Crossover.*—The solid lines shown in Fig. 4 are fits to  $T_{1/e} = b(J_{\perp}/J)^k$ , where amplitude  $b$  and the power law exponents  $k$  are free fit parameters. The fitted exponents are plotted in Fig. 9 as a function of interactions. Note that the exponents for all the interacting cases are negative with absolute values much smaller than unity. The exponents depend non-monotonously on the interaction strength, resembling the shape of the 2D curve in Fig. 5.